Statistical Analysis of Topographic and Climatic Controls and Multispectral Signatures of Rock Glaciers in the Dry Andes, Chile (27°–33°S)

A. Brenning [1]* *and G. F. Azócar* [1,2]

[1] Department of Geography and Environmental Management, University of Waterloo, Ontario, Canada
[2] Escuela de Geografía, Universidad de Chile, Santiago, Chile

ABSTRACT

The dual nature of rock glaciers as ice-rich mountain permafrost and sediment storage systems results in a combination of geomorphic processes and energy balance components controlling their distribution. We use the generalised additive model (GAM), a semi-parametric nonlinear method, to empirically analyse environmental controls and spectral characteristics of rock glaciers in the dry Andes of Chile based on presence/absence data at random point locations and predictor variables derived from digital elevation models and Landsat data. A combination of nonlinearly transformed local and catchment-related terrain attributes (especially local and catchment slope and potential incoming solar radiation, PISR) characterises the geomorphic and climatic niche of rock glaciers. The influence of (latitude adjusted) relative PISR varies with mean annual air temperature (MAAT): high-PISR sites are favourable for rock glacier development at lower MAATs and low-PISR sites at higher MAATs. TM/ETM+ band 6 (thermal infrared) is an additional nonlinear predictor. The combination of topographic, climatic and multispectral data in a GAM achieves an excellent general discrimination (area under the ROC curve 0.87 on the model domain and 0.94 overall). In automatic rock glacier detection at a sensitivity of 70 per cent, this model achieves a false-positive rate (FPR) of 6.0 per cent overall and 12.8 per cent on the model domain (bootstrap estimates: 7.9% and 16.8%). Dropping the multispectral data significantly increases the bootstrapped FPR by 36 per cent. Thus, the fusion of multisource data using modern nonlinear classification techniques is a promising step towards automatic rock glacier detection. Copyright © 2009 John Wiley & Sons, Ltd.

KEY WORDS: generalised additive model; logistic regression; digital elevation model; terrain analysis; rock glacier; Andes

INTRODUCTION

The complex topographic and climatic controls on rock glacier occurrence and characteristics have been a focus of rock glacier research since its early days (Wahrhaftig and Cox, 1959; Frauenfelder *et al.*, 2003; Janke, 2005; Brenning and Trombotto, 2006; Brenning *et al.*, 2007; Johnson *et al.*, 2007). The complexity of these relationships is a result of the dual nature of rock glaciers as ice-rich mountain permafrost and sediment storage systems. As permafrost features, rock glacier occurrence is influenced by topoclimatic factors such as air temperature and solar radiation that affect their energy balance. Rock glaciers as sediment storage systems depend on post-glacial talus production and transport, which are related to topographic characteristics of rock glacier sites and talus sheds (Brenning and Trombotto, 2006).

Modern statistical analysis techniques are powerful tools that provide insight into the environmental factors that are empirically related to rock glacier distribution. Logistic regression (Brenning and Trombotto, 2006; Janke, 2005) and more recently the more flexible generalised additive model (GAM; Hastie and Tibshirani, 1990; Brenning *et al.*, 2007) have been used for this purpose. These analyses have been the starting point for the development and comparison of different algorithms for automatic, multisource rock glacier detection with a combination of terrain attributes and remote-sensing variables (Brenning, 2009). Disentangling the relationships between rock glacier occurrence and topographic, climatic and spectral patterns will therefore not only enhance our understanding of rock glaciers within the mountain environment, but it will also improve automatic mapping algorithms to be developed for efficiently mapping rock glaciers. Advances in automatic rock glacier detection

* Correspondence to: A. Brenning, Department of Geography and Environmental Management, University of Waterloo, 200 University Avenue West, Waterloo, Ontario, Canada N2L 3G1.
E-mail: brenning@uwaterloo.ca

may help improve algorithms for mapping glaciers – especially debris-covered ones – from space as intended by initiatives such as the Global Land Ice Measurements from Space project (GLIMS; Kargel *et al.*, 2005). While rock glaciers are usually not included in glacier inventories, the detection of debris-covered parts of glaciers poses a major challenge that is related to the problem of rock glacier detection because the two spectral signatures are similar (Gratton *et al.*, 1990; Paul *et al.*, 2004; Bolch and Kamp, 2006; Brenning, 2009).

The objective of this paper is to analyse the influence of topographic and climatic variables on rock glacier distribution in the dry Andes, and to determine to what degree multispectral Landsat TM/ETM+ data can improve rock glacier detection in this arid environment. The GAM and logistic regression are used (see Brenning, 2009). This builds on the results by Azócar and Brenning (2009), who statistically estimated rock glacier areas and water equivalents in the dry Andes, and characterised their distribution and geomorphic and hydrological importance in the context of regional climatic setting and the scarcity of glaciers in the area. The reader is referred to this companion paper for a geographical characterisation of the study area.

DATA AND METHODS

Statistical estimation based on air photo interpretation at random point locations is an efficient method for the quantification of rock glacier area and water equivalent (Brenning, 2005), and GAMs are flexible tools for the analysis and prediction of rock glacier distribution (Brenning *et al.*, 2007; Brenning, 2009). In this application of GAMs and logistic regression models to analyse rock glacier distribution in the dry Andes, we use a learning set of random locations generated and presented by Azócar and Brenning (2009), where 72 out of a total of 5308 samples were classified as rock glacier locations based on air photo interpretation. The samples are spread over an area of $10\ 616\,km^2$ above the approximate lower limit of rock glacier distribution. Of the original 5308 point locations, the present data exclude 72 points where air photos or suitable satellite imagery were unavailable, and four points that were found to be east of the Chile-Argentina border. Moreover, our analysis focuses on 2485 samples (corresponding to 48% of the study area) that passed a first screening step which excludes topographically clearly unsuitable areas according to an unsuitability score defined by Azócar and Brenning (2009). The score is based on thresholds on the catchment-area size ($0.1–3.16\,km^2$ are suitable), the catchment slope (must be $\geq 15°$) and the local slope (must be $\leq 45°$); in addition, the elevation must lie between the extreme upper and lower limits of rock glacier occurrence identified by Brenning (2005) and refined by Azócar and Brenning (2009). We refer to this more focused area as the *model domain*.

All statistical analyses are performed within the data analysis environment R. The GAM is implemented in R's 'gam' package. Terrain attributes are calculated with SAGA GIS and R's 'RSAGA' package. A digital elevation model (DEM) from the Shuttle Radar Topography Mission (SRTM version 3 from Consultative Group for International Agriculture Research Consortium for Spatial Information (CGIAR) with filled gaps, vertical standard error $\pm 15–16$ m, Kääb, 2005; resolution $3''$, projected and resampled to a resolution of 90 m) is used for all analyses.

Generalised Additive and Linear Models

The GAM is a flexible yet interpretable model that has been successfully used in periglacial geomorphology, including rock glacier distribution modelling (Luoto and Hjort, 2005; Hjort and Luoto, 2006; Brenning *et al.*, 2007; Brenning, 2009). It extends the generalised linear model (GLM) using a combination of linear and nonlinear terms to represent predictor variables (Hastie and Tibshirani, 1990), which is important in this context (compare Brenning *et al.*, 2007, with Brenning and Trombotto, 2006).

In the case of a binary response variable Y such as the presence ($Y=1$) versus absence ($Y=0$) of rock glaciers, we model the probability $\pi(\mathbf{x})=P(Y=1|\mathbf{x})$ of rock glacier occurrence conditional on a vector of predictor variables $\mathbf{x}=(x_1,\ldots,x_p)^{\mathrm{T}}$ characterising local site conditions and regional climatic trends. In this situation, the GAM represents the *logit* of this conditional probability as an additive function of the predictors:

$$\mathrm{logit}(x) = f_1(x_1) + \ldots + f_p(x_p),$$

where the log-odds or logit is defined as:

$$\mathrm{logit}(\mathbf{x}) = \ln(\mathrm{odds}(\mathbf{x})) = \ln[\Pi(\mathbf{x})/(1 - \Pi(\mathbf{x}))],$$

and where the functions $f_1,\ldots,f_p$ are possibly nonlinear functions of the predictor variables. These transforms can be obtained using, for example, smoothing splines (here of two equivalent degrees of freedom), or local polynomial regression (Hastie and Tibshirani, 1990), though individual predictors can still be modelled linearly.

We constructed three GAMs with different sets of predictor variables:

1. only terrain attributes and position variables representing topographic and climatic conditions (model abbreviated as GAM-TA),
2. only multispectral remote-sensing data (GAM-RS), and
3. both sets of variables (GAM-TA-RS).

We fitted the GAM-TA and GAM-RS by stepwise-forward variable selection starting with an empty model. The GAM-TA-RS was then built by combining the predictor variables in the GAM-TA and GAM-RS. A stepwise variable selection on the full set of predictor variables was not possible because of memory limitations.

The topographic and climatic predictors considered in model construction are described below. Each variable could be included as a linear variable (as in logistic regression), as a nonlinearly transformed one, or not at all. Variable selection is based on the Akaike Information Criterion

(AIC), which penalises for the number of variables in a model and thus helps avoid overfitting, keeping the model small and interpretable. This strategy not only produces good analytical models, but also models with excellent predictive capabilities in rock glacier detection (Brenning, 2009).

We also compare the results of the GAM with logistic regression (henceforth referred to as GLM), i.e. the special case of an additive model with linear influences of the predictor variables. This allows us to interpret rock glacier distribution in a parametric framework, and to assess whether ignoring the (possibly limited) nonlinearities in predictor variables results in an appreciable loss of goodness-of-fit.

Model Evaluation

The overall performance of the GAM and GLM is measured by the area under the receiver-operating characteristic (ROC) curve (AUROC). It can range between 0.5 (no separation) and 1.0 (complete separation of presence and absence by the model). The ROC curve represents all possible combinations of sensitivities (percentage of observed positives that are correctly predicted as such, or true-positive rate) and specificities (true-negative rate) that can be achieved by a probability model.

Effective rock glacier detection requires a large percentage of actual rock glaciers to be correctly predicted (i.e. high sensitivity). We use a fixed high sensitivity of 70 per cent, at which we measure the false-positive rate (FPR) of a classifier. High sensitivity allows us to identify most rock glacier grid cells, and to detect almost all rock glacier objects at least partly, as discussed below. The overall misclassification error rate (overall percentage of samples that is misclassified) of the classifier would not be an appropriate error measure because false-positive and false-negative predictions must be weighted differently (Brenning, 2009).

In addition to measuring the AUROC and FPR on the training set, we also perform bootstrap error estimation in order to obtain unbiased estimates of the performance of the GAM and GLM. Bootstrapping is based on approximating the data-generating distribution by empirical distribution of the data set. Independent training and test sets can thus be obtained by drawing objects with replacement from the data set. We use 100 bootstrap training sets and the same number of bootstrap test sets, each drawn independently from the learning set. Resampling is stratified with respect to the response variable in order to maintain a constant rock glacier density. This results in 100 independent estimates of AUROC and FPR for each classification method. The different GAM and GLM models obtained on each of the bootstrap training sets by stepwise variable selection are examined further in order to determine variable selection frequencies as an indicator of variable importance.

We statistically test pairwise differences in bootstrap estimates of AUROC and FPR on equality using a Wilcoxon signed rank test with Bonferroni correction for multiple comparisons (15 pairwise tests for AUROC and FPR, respectively) to control the familywise error rate at the 5 per cent level. Effects of potential spatial autocorrelation on statistical inference and bootstrap estimation can be disregarded at the present sampling density of $0.5 \, \mathrm{km}^{-2}$.

The GAM using terrain attributes and remote-sensing data (GAM-TA-RS) is also used for predicting a rock glacier probability map for the entire study area and further east into the Argentine Andes. A median filter is applied to reduce noise in the prediction map and to obtain more compact rock glacier objects.

Predictor Variables.

In order to effectively characterise the geomorphic niche of rock glaciers, we use a set of SRTM-derived positional variables and terrain attributes that are related to local topographic and climatic site conditions, catchment-area characteristics controlling talus supply and regional climatic trends. In addition, Landsat TM/ETM+ spectral and derived data are used. Table 1 gives an overview of all predictor variables and univariate descriptive statistics for assessing the utility of individual variables. Variable importance in the GAMs and GLMs is measured in terms of deviance reduction and bootstrap variable selection frequency.

Topographic and Climatic Variables

Mean annual air temperature (MAAT) represents regional-scale latitudinal variation and is based on the modern 0°C isotherm of MAAT synthesised by Brenning (2005) based on several primary data sources, and an assumed lapse rate of 0.65°C per 100 m. In addition to the estimated MAAT, latitude itself and an interaction term of MAAT and latitude are also considered in model building because the effect of temperature itself and confounding effects may change across several hundred kilometres in a north-south direction (see Azócar and Brenning, 2009).

Morphometric properties of rock glaciers can be measured by terrain attributes representing slope angle, plan and profile curvature, and an important driver of the surface energy balance can be captured by PISR. PISR, as an annual sum, is represented as an index relative to the average PISR at the same latitude, resulting in values mostly between 0.8 and 1.2 (i.e. local topographic conditions account for a departure of ±20% from the regional average). This index allows us to separate latitudinal from topographic variation in radiation. The interaction term of relative PISR and MAAT is considered as a potential additional predictor variable because such an interaction had a significant influence on rock glacier distribution in the Andes of Santiago (Brenning and Trombotto, 2006). The same study also found a significant effect of plan curvature.

The size of the catchment area is a potentially important predictor variable as it is related to the intensity and type of talus supply processes (Frauenfelder *et al.*, 2003; Janke and Frauenfelder, 2008; Azócar and Brenning, 2009). We calculate it with the Multiple Flow Direction algorithm. A related predictor variable is the height of the catchment

Table 1 Descriptive statistics of the morphometric and multispectral predictor variables used for modelling rock glacier distribution

Variable	Unit	Model domain			Entire area
		Non-rock glaciers: Mean (Std dev.)	Rock glaciers: Mean (Std dev.)	AUROC	AUROC
MAAT	°C	−1.04 (1.86)	−1.15 (1.79)	0.51	0.58
Latitude	°S	30.57 (1.58)	30.85 (1.64)	0.54	**0.65**
Latitude × MAAT		−29.9 (56.7)	−34.0 (53.6)	0.51	0.57
Local slope	°	24.8 (8.3)	**21.1 (8.7)** ***	**0.63**	0.50
Catchment slope	°	25.0 (5.4)	**28.1 (4.1)** ***	**0.68**	**0.78**
Log_{10} catchment area	$log_{10}(m^2)$	4.72 (0.47)	**5.11 (0.49)** ***	**0.73**	**0.74**
Log_{10} catchment height	$log_{10}(m)$	1.98 (0.42)	**2.31 (0.34)** ***	**0.74**	**0.78**
Plan curvature	°/100 m	0.43 (11.4)	**−3.42 (8.81)** **	**0.61**	**0.63**
Profile curvature	°/100 m	−0.70 (9.34)	**−4.43 (9.76)** **	**0.60**	**0.65**
Relative PISR		0.99 (0.06)	1.00 (0.06)	0.55	0.52
Relative PISR × MAAT		−1.05 (1.85)	−1.21 (1.75)	0.52	0.57
TM/ETM+ Band 1	DN	48.9 (12.1)	51.3 (12.9)	0.56	0.51
TM/ETM+ Band 2	DN	47.2 (15.0)	49.9 (14.3)	0.56	0.51
TM/ETM+ Band 3	DN	60.3 (22.6)	63.1 (21.2)	0.54	0.51
TM/ETM+ Band 4	DN	70.5 (27.4)	72.4 (25.4)	0.52	0.54
TM/ETM+ Band 5	DN	53.1 (25.0)	54.2 (23.1)	0.52	0.53
TM/ETM+ Band 6	DN	79.9 (44.8)	69.0 (38.2)	0.55	0.57
TM/ETM+ Band 7	DN	50.2 (17.2)	52.8 (15.7)	0.56	0.51
NDVI		0.073 (0.033)	**0.066 (0.028)** *	0.57	**0.62**
NDSI		−0.02 (0.13)	−0.01 (0.15)	0.50	0.55
Log_{10} band ratio 4:5		0.14 (0.08)	0.14 (0.10)	0.53	0.51

*, **, *** Differences in location parameter are significant at the 5 per cent, 1 per cent and 0.1 per cent levels, respectively (Mann-Whitney test with normal approximation). Abbreviations are defined in the text. Significant test results and AUROC values of at least 0.60 are highlighted in bold.

area. Both are highly skewed and are therefore log-transformed. Catchment slope controls the effectiveness of gravitational processes in providing talus to a rock glacier.

Multispectral Remote-Sensing Data

Among the Landsat TM/ETM+ variables that may be important for distinguishing between rock glaciers and the various types of non-rock glacier surfaces are the normalised-differences vegetation index (NDVI), the thermal band (band 6), the normalised-differences snow index (NDSI) and the TM/ETM+ 4:5 band ratio (Hall *et al.*, 1987; Williams *et al.*, 1991; Sidjak and Wheate, 1999; Paul *et al.*, 2004; Brenning, 2009). The NDSI is the normalised difference of TM/ETM+ bands 2 and 5, which has been effective in distinguishing snow from bright soil, vegetation and rock based on the difference between reflection of visible radiation and absorption of middle infrared by snow (Hall *et al.*, 1995; Sidjak and Wheate, 1999).

Spectral and derived variables were obtained from a combination of several orthorectified Landsat TM and ETM+ images (TM path/row 233/83 of 17 March 1989; TM 233/82 of 13 April 1990; ETM+ 233/81 of 21 March 2002; TM 233/80 of 2 April 1986; ETM+ 233/79 of 26 November 2000; all retrieved from the Global Land Cover Facility at the University of Maryland, http://www.landcover.org/). Random influences on spectral data due to different acquisition dates were removed by per-band linear transformations. Transformation coefficients were estimated

in overlapping areas by quantile regression of the median, a method that is resistant to outliers and noise (Koenker, 2005). Simple regression of corresponding bands of adjacent images provides an acceptable goodness-of-fit in most cases ($R^2 \geq 68\%$). Transformations based on regression models with multiple bands as predictors were applied in five cases where the univariate R^2 was between 7 per cent and 57 per cent. Four of these related to the difference between images 233/78 and 233/79. The multiple-variable band transformations increased these R^2 values to 53–76 per cent.

We use the transformed digital number (DN) of each spectral band (bands 1–7; the panchromatic band of ETM+ is omitted) as potential predictor variables and, in addition, the NDVI, the NDSI and the log-transformed ratio of bands 4 and 5 (Table 1).

RESULTS

Exploratory Data Analysis

After applying the unsuitability score to limit the sample to the model domain, univariate AUROC values indicated that a variety of local and catchment-related terrain attributes and, to a lesser extent, selected multispectral variables could be useful to discriminate rock glacier presence and absence (Table 1). Catchment height and area were the strongest univariate predictors (AUROC > 0.70 on the model domain), followed by catchment slope, local slope, and

plan and profile curvature (AUROC ≥ 0.60). Differences in the location parameters of these variables were also statistically significant (Mann-Whitney test, 5% significance level).

The NDVI and Landsat TM/ETM+ bands 1, 2 and 6 were the most relevant univariate remotely sensed predictors of rock glacier presence, although with weak univariate discriminatory power (AUROC ≥ 0.55). The NDVI, how-ever, was the only remotely sensed variable with a significant difference between presence and absence samples in the location parameter. Reported differences in the predictive power of the other remotely sensed variables may be due to random variation. Variables that appear to be of little importance here, however, may still be important in nonlinear multiple variable models.

Most of the TM/ETM+ bands were strongly intercorre-lated, with Spearman correlation coefficients >0.80 between all bands except the thermal infrared (band 6), and 0.60–0.69 between band 6 and the other bands. The NDSI was strongly correlated with band 5 (Spearman correlation −0.87) and with the ratio of bands 4 and 5 (0.86), and less with bands 3, 4 and 7 and the NDVI (Spearman correlation −0.60 to −0.68). The correlation of the NDVI with other variables was strongest for the NDSI (−0.65), and the 4:5 band ratio was strongly correlated with NDSI (0.86) and band 5 (−0.67).

All Spearman correlations between TM/ETM+ variables and terrain attributes ranged between −0.50 and +0.50. The height and size of the contributing area were the most strongly intercorrelated terrain attributes (Spearman corre-lation 0.92). The pairs latitude/MAAT and local slope/catchment slope followed with correlations of 0.66, while all other pairs of terrain attributes had correlations between −0.60 and +0.60 (mostly −0.30 to +0.30).

GAM and GLM Variable Selection and Importance

The GAM that used only terrain attributes (GAM-TA) included, after stepwise variable selection based on the AIC, five variables: local and catchment slope, log-catchment height, MAAT and relative solar radiation (Table 2). The latter two were combined by a two-dimensional, nonlinear interaction term representing a solar radiation influence that differed between colder and more temperate sites. In addition to this interaction, both slope variables were included as nonlinearly transformed predictors.

The remote sensing-based GAM (GAM-RS) contained Landsat bands 2 and 6 (thermal infrared), both after nonlinear transformation (Table 2). The bootstrapped variable selection frequencies clearly indicate that the variables selected by our models GAM-TA and GAM-RS

Table 2 GAMs and GLMs relating rock glacier occurrence to terrain attributes (GAM-/GLM-TA), Landsat TM/ETM+ data (GAM-/GLM-RS) and both sets of predictors (GAM-/GLM-TA-RS)

Model	Variable	GAM				GLM		
		Transformed [a]	p-Value of transformation	p-Value of effect	Deviance reduction	Coefficient	Standard error	p-Value
GAM-/GLM-TA	Intercept	(No)				−6.70	2.75	0.014 *
	MAAT	No[b]		<0.001 ***	0.00[b]	2.62	1.03	0.011 *
	Local slope	Yes	0.097	<0.001 ***	34.0	−0.11	0.02	<0.001 ***
	Catchment slope	Yes	0.008 **	<0.001 ***	41.9	0.19	0.03	<0.001 ***
	Log_{10} catchment height	No		0.068	3.3	0.88	0.46	0.059
	Relative PISR	—[b]	—[b]	—[b]	—[b]	−1.41	2.46	0.566
	Relative PISR × MAAT	Yes	0.005 **	0.008 **	18.1	−2.69	1.03	0.009 **
GAM-/GLM-RS	Intercept	(No)				−0.92	0.85	0.276
	Band 2	Yes	0.008 **	<0.001 ***	14.9	0.03	0.01	<0.001 ***
	Band 6	Yes	0.001 **	<0.001 ***	34.4	−0.03	0.01	<0.001 ***
GAM-/GLM-TA-RS	Intercept	(No)				−6.18	2.89	0.032 *
	MAAT	No[b]		<0.001 ***	0.00[b]	2.68	1.03	0.009 **
	Local slope	Yes	0.080	<0.001 ***	28.9	−0.11	0.02	<0.001 ***
	Catchment slope	Yes	0.008 **	<0.001 ***	39.8	0.19	0.04	<0.001 ***
	Log_{10} catchment height	No		0.115	2.5	0.93	0.47	0.047 *
	Relative PISR	—[b]	—[b]	—[b]	—[b]	−1.47	2.53	0.560
	Band 2	Yes	0.019 *	0.008 **	9.6	0.03	0.01	0.004 **
	Band 6	Yes	0.002 **	0.001 **	14.4	−0.01	0.01	0.116
	Relative PISR × MAAT	Yes	0.004 **	0.007 **	18.2	−2.70	1.03	0.009 **

*, **, *** Hypothesis tests are significant at the 5 per cent, 1 per cent and 0.1 per cent levels, respectively (χ^2 score test).
[a] Indicates whether a variable is included in a GAM as a linear variable or nonlinearly transformed.
[b] MAAT and relative PISR are included in the GAMs' non-parametric bivariate loess smoother representing their interaction term. MAAT was separately selected by automatic variable selection. Abbreviations are defined in the text.

Table 3   Variable selection frequencies over 100 bootstrap replications for GAMs and GLMs combining terrain attributes and remote-sensing variables

Variable	GAM			GLM
	Linear	Transformed	Total	Total
Catchment slope	0	100	100	100
Local slope	38	62	100	100
TM/ETM+ Band 6	0	100	100	65
Relative PISR × MAAT	21	64	85	6
Log_{10} catchment height	30	36	66	66
Latitude × MAAT	0	57	57	7
TM/ETM+ Band 2	2	49	51	45
MAAT	40	0	40	27
Profile curvature	19	15	34	29
Relative PISR	24	8	32	27
NDVI	4	26	30	9
TM/ETM+ Band 1	11	17	28	21
Log_{10} band ratio 4:5	9	8	17	48
TM/ETM+ Band 5	4	13	17	19
TM/ETM+ Band 3	11	6	17	19
TM/ETM+ Band 4	15	2	17	10
Plan curvature	4	9	13	28
TM/ETM+ Band 7	2	9	11	16
Log_{10} catchment area	2	9	11	10
Latitude	8	2	10	56
NDSI	4	4	8	27

Variables are ranked according to the total (linear and transformed) selection frequency in the GAM. Abbreviations are defined in the text.
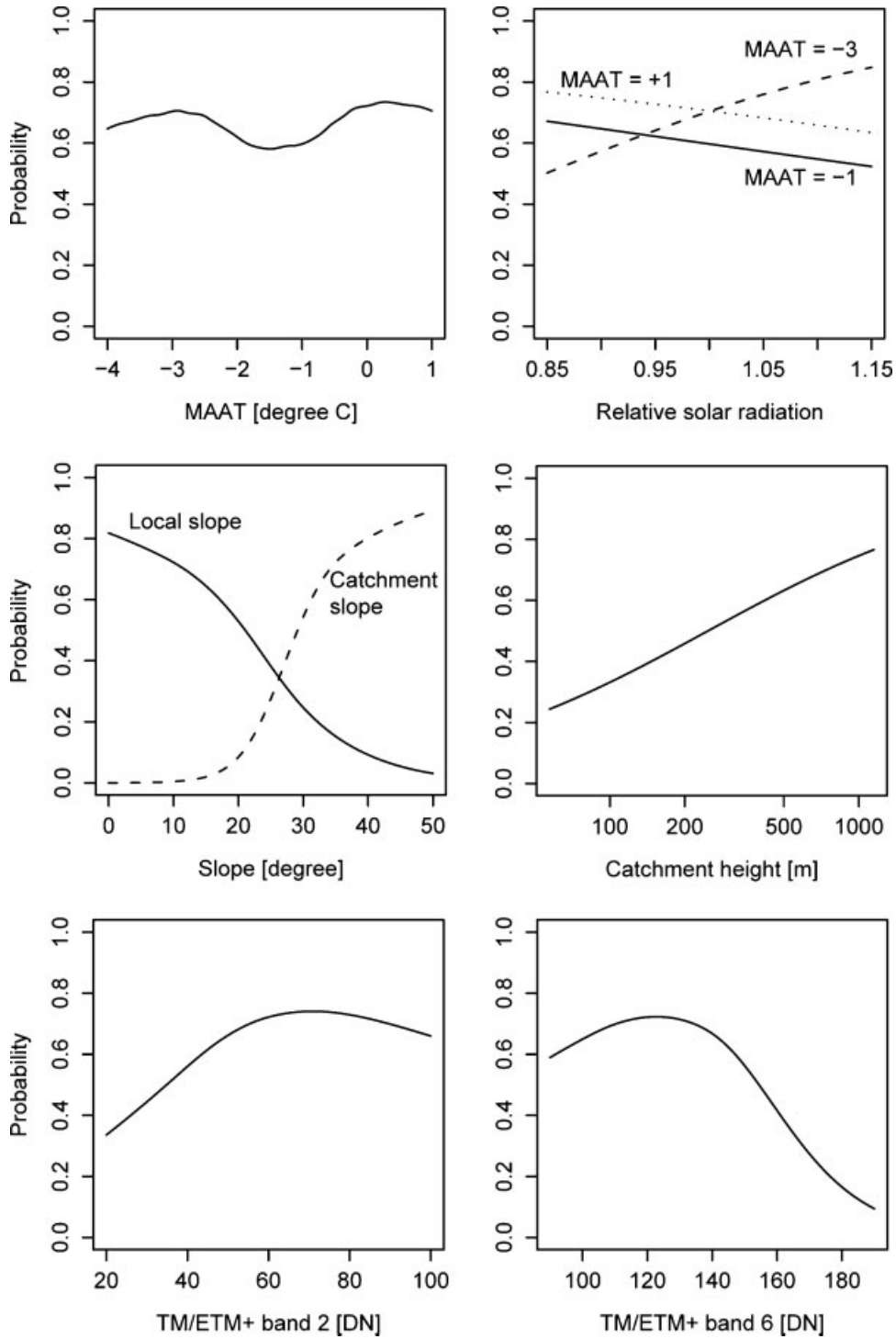
Figure 1   Illustration of rock glacier probabilities predicted by the GAM-TA-RS model. The other variables are fixed at the following values: MAAT −1°C, local slope 10°, catchment slope 35°, catchment height 500 m, relative solar radiation 1.00, TM/ETM+ band 2 DN 60, band 6 DN 120. Abbreviations are defined in the text.

Table 4   Predictive performance of GAMs and GLMs on the training set and using bootstrapping

Model	Model domain				Entire study area	
	AUROC [%]		FPR [%] at 70% sensitivity		AUROC [%]	FPR [%] at 70% sensitivity
	Training set	Bootstrap	Training set	Bootstrap	Training set	Training set
GAM-TA	82.5	81.6 (2.5)	20.4	22.9 (5.4)	91.8	9.6
GAM-RS	70.6	68.8 (7.8)	40.6	42.2 (8.9)	86.2	19.0
GAM-TA-RS	**86.4**	**85.0 (2.3)**	**12.8**	**16.8 (4.7)**	**93.6**	**6.0**
GLM-TA	80.2	79.5 (2.6)	22.8	25.3 (6.0)	90.7	10.8
GLM-RS	66.0	63.7 (7.1)	44.8	48.3 (7.0)	84.0	21.0
GLM-TA-RS	81.9	81.6 (2.8)	18.8	20.9 (5.3)	91.5	8.8

The models include terrain attributes (TA), Landsat TM/ETM+ remote-sensing data (RS) and both sets of predictors (TA-RS). Except for the comparison GLM-TA-RS vs. GAM-TA, all pairwise differences in bootstrapped AUROC values and FPRs are statistically significant at the 5 per cent level (p-values <0.1% after Bonferroni correction for multiple comparisons). FPR = False-positive rate (1 – specificity) at a sensitivity of 70 per cent. Other abbreviations are defined in the text. Best results are highlighted in bold.

are robust with respect to changes in the training set (Table 3).

The transformation functions used by the combined model (GAM-TA-RS) are displayed in Figure 1, and the results of hypothesis tests (χ^2 score test, 5% significance level) on the significance of a variable or of its nonlinear transformation (as opposed to the alternative linear term) are summarised in Table 2. All variables except the log-catchment height contribute significantly to the GAM-TA-RS model. Of the five nonlinear terms in the models, the transformations of catchment slope, bands 2 and 6, and the interaction of solar radiation and MAAT are supported by significance tests at the 5 per cent level, while local slope could be represented by linear terms.

As a measure of variable importance we first used the change in deviance that is associated with removing each variable from the GAMs (Table 2). In the GAM-TA-RS, the nonlinearly transformed catchment slope (deviance reduction 39.8) was followed by the transformed local slope (28.9) as the most important predictor variables. The interaction of relative solar radiation with MAAT, and TM/

ETM+ thermal infrared band 6 followed (deviance reduction 18.2 and 14.4, respectively), while the other variables contributed less to the model fit (band 2: 9.6; catchment height: 2.5). (The inclusion of MAAT resulted in no change in deviance because its influence is captured by the interaction term of MAAT with relative solar radiation.)

The bootstrapped variable selection frequencies in the GAM mostly agreed with observations based on the deviance (Table 3). Catchment slope, local slope and TM/ETM+ band 6 were included in all GAMs trained on different bootstrap sets, with catchment slope and band 6 consistently being used with nonlinear transformations. Local slope also mostly required a nonlinear transformation. The interaction of solar radiation and MAAT found its way into the GAM in 85 per cent of the models, mostly using a nonlinear transformation. Catchment height (66% frequency) predominated over its confounder catchment area (11%). The interaction of latitude and MAAT (57%), TM/ETM+ band 2 (51%) and MAAT (40%) also had moderate selection frequencies. Low selection frequencies may be
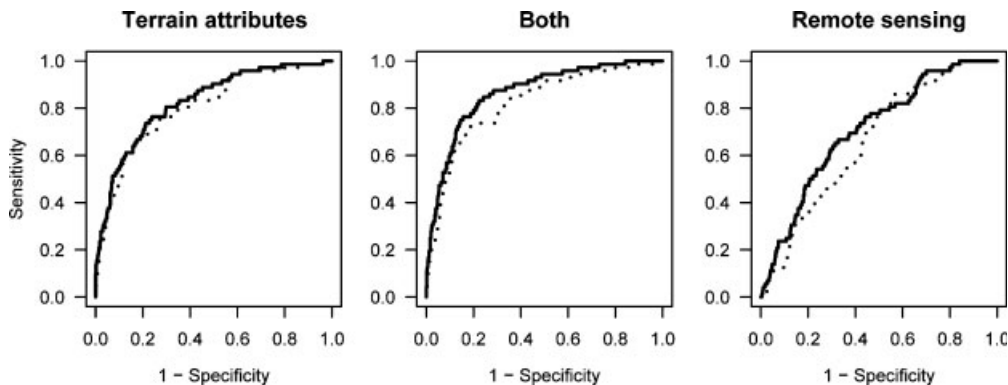

Figure 2   ROC curves of rock glacier prediction in the model domain using the GAM (solid lines) and the GLM (dotted) with remote-sensing data, terrain attributes and the combination of both. AUROCs and FPRs (1 – specificity) at a sensitivity of 70 per cent are displayed in Table 3. Abbreviations are defined in the text.

interpreted as overfitting to random patterns in individual bootstrap training sets.

The nonlinearities of the transformations were mostly moderate (Figure 1). A GLM may therefore provide a reasonable approximation to the GAM. The results of fitting GLMs (GLM-TA, GLM-RS, GLM-TA-RS) with the same predictors as the corresponding GAMs are displayed in Table 2. The results of hypothesis tests are similar to those obtained with the GAM; however, TM/ETM+ band 6 was not significant in the GLM-TA-RS. Bootstrapped variable selection frequencies in the GLM were somewhat different

from the GAM. In particular, the complex, considerably nonlinear interactions between PISR and MAAT and between latitude and MAAT, which were identified by the GAM, were not captured by the GLM because it can only include linear interactions unless nonlinear transformations are explicitly specified by the modeller.

Predictive Performance

The predictive performance measures of AUROC and the FPR at a sensitivity of 70 per cent indicate that the combined GAM-
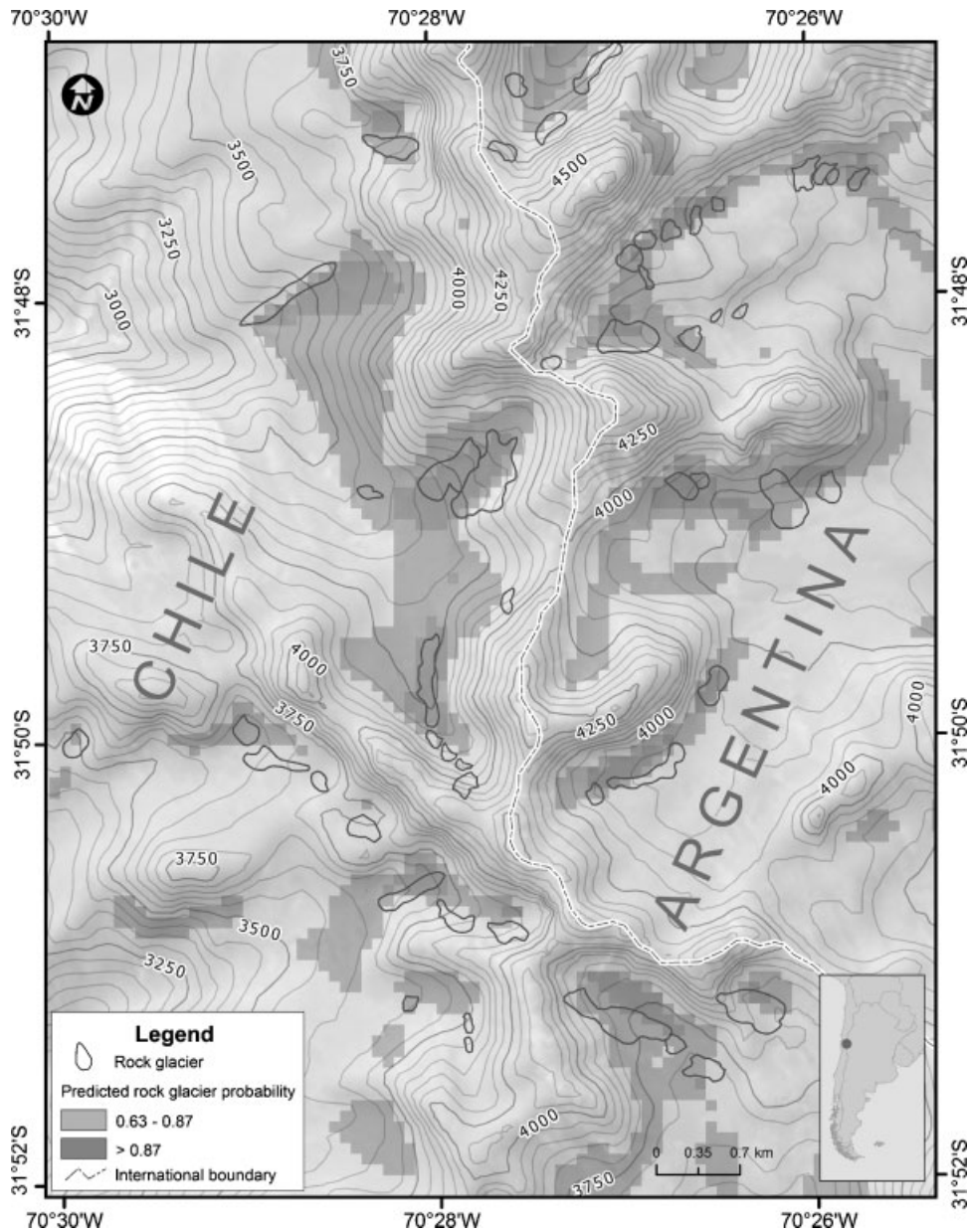

Figure 3   Rock glacier prediction generated by the GAM-TA-RS in a sample area at 31°50′S. Rock glacier outlines based on air photo interpretation (GEOTEC flight, air photos 2405-07). Probability thresholds represent area-preserving prediction (0.87) and predictions corresponding to a sensitivity of 70 per cent (0.63). Abbreviations are defined in the text.

TA-RS is an important improvement over the GAM-TA and especially the GAM-RS; the latter model is clearly not useful for practical purposes (Table 4; Figure 2). The AUROC of the GAM-TA-RS (86.4% on the training set and 85.0% with bootstrap estimation) is somewhat better than the AUROC of its submodel the GAM-TA (82.5% and 77.8%, respectively), and it outperforms the GAM-TA more clearly in rock glacier detection at high sensitivities (so-called early detection) as it reduces the FPR from 20.4 per cent (bootstrap: 22.9%) to 12.8 per cent (16.8%) on the model domain and from 9.6 per cent to 6.0 per cent if projected to the entire study area (bootstrap: reduction from 10.8% to 7.9%). At an average specific density of rock glaciers of 1.4 per cent across the entire study area, the GAM-TA-RS achieved a positive predictive value of 14 per cent on the training set (bootstrap: 11.0%), that is 14 per cent of the predicted rock glacier areas (at the 70%-sensitivity threshold) are indeed rock glaciers, compared to a rock glacier density of 1.4 per cent overall and 2.9 per cent in the model domain.

The bootstrapped predictive performance of the GLM-TA-RS model was not statistically distinguishable from the performance of the GAM-TA without remotely sensed variables, but the GAM-TA-RS had a statistically significant advantage over all other models in terms of bootstrapped AUROC and FPR (Table 4).

At the selected sensitivity of 70 per cent, 21 of the 72 rock glaciers in the data set were missed by the rock glacier prediction of the GAM-TA-RS. However, ten of these false-negative predictions of rock glacier point samples were missed by only one pixel. Thus, allowing for a one-pixel tolerance increases sensitivity to 84.7 per cent, and a two-pixel tolerance results in a 93.1 per cent sensitivity of the GAM-TA-RS on the training set. This indicates that for the proposed detection procedure, the GAM-TA-RS is more effective than what would be expected from a nominal 70 per cent sensitivity.

Figure 3 shows a map of the predicted probabilities of rock glacier occurrence in a sample area at $31°$ $50'$S on the border between Chile and Argentina, and a comparison with manual mapping results based on aerial photographs of 1997 (GEOTEC flight). In this area with 52 individual rock glaciers (46 landforms $>0.01\,km^2$, and seven $>0.1\,km^2$), the 70 per cent-sensitivity threshold of the entire study area resulted in an observed local sensitivity of 66.8 per cent and a local FPR of 15.1 per cent, which is less accurate than the performance on the training set but close to the bootstrap error estimate (Table 4). On the other hand, the seven most significant rock glaciers ($>0.1\,km^2$) were all detected because they are at least partly covered by predicted rock glacier grid cells. Some 82.6 per cent of rock glaciers $>0.01\,km^2$ were detected, and 75.0 per cent of all rock glaciers in this area. The areas of false-positive predictions were often in areas with moraines, or they corresponded to small talus cones and rock faces that are not accurately represented by the SRTM DEM.

DISCUSSION

Topographic and Climatic Niche of Rock Glaciers

The topographic and climatic niche of rock glaciers in the dry Andes is mainly characterised by catchment slope, local slope, MAAT and an altitudinally varying influence of PISR. Catchment-area size is a surrogate of the overall talus production, which is another important control on rock glacier development. This surrogate variable is implicitly included in our model through the unsuitability score, and through its confounder, catchment-area height. The influence of MAAT comes into play in the GAM-TA-RS through the upper and lower limits of rock glacier distribution that are reflected by the unsuitability score, and through the interaction with solar radiation. At an average relative solar radiation of 1.0, however, there is no influence of MAAT on rock glacier abundance within this altitudinal belt since the coefficients almost cancel each other out (2.618–2.685 = 0.067). The bootstrap variable selection frequencies suggest that the interaction of latitude and MAAT could provide further valuable information, possibly by adjusting for latitudinally varying altitudinal belts or inaccuracies in the lower and upper rock glacier limits adopted from previous studies.

The optimal topographic niche of rock glaciers within the altitudinal belt of their general distribution (Azócar and Brenning, 2009) has a local slope angle of up to 20–22° and a talus shed with an average slope angle of more than 30–33°. Large altitudinal differences within the catchment area tend to be favourable. These talus shed characteristics allow for effective gravitational talus supply by rockfall, debris flows and avalanches (Frauenfelder et al., 2008) and are consistent with a mean contributing-area slope of 37° (standard deviation 6–7°) found by Janke and Frauenfelder (2008) in the Colorado Front Range. The optimal rock glacier slope angle of 20–22° agrees well with the observation of a mean rock glacier slope angle of 21–22° (standard deviation 6–7°) in the Front Range and a range of slope angles from 10 to 27° (outlier 6°) in different areas worldwide (Janke and Frauenfelder, 2008). Data from previous studies also show that rock glacier talus sheds rarely exceed $\sim3\,km^2$ (Brenning, 2005; Brenning et al., 2007), as represented by our unsuitability score. This reflects the general size limits of rock glaciers (generally $\leq2\,km^2$; Brenning, 2005), as well as river discharge and erosion in watersheds of this size even in the dry Andes.

The interaction of MAAT and relative PISR in our models indicates that high solar radiation has a positive effect on rock glacier probability at negative MAATs and a negative effect at low elevations. This is particularly evident in the GLM (GLM-TA, Table 2). At $+1°C$ MAAT, a change in relative solar radiation by 0.12 (i.e. two standard deviations, see Table 1) results in a 63 per cent increase in the odds of rock glacier occurrence, while the same difference between shady and more exposed locations at $-1°C$ would have the opposite effect according to our model GLM-TA. A significant contribution of an interaction of elevation and solar radiation was also found by Brenning and Trombotto (2006) in the Andes at $33°$–$34.5°$S, where the influence of

solar radiation also changes its sign at the regional 0°C isotherm altitude.

PISR and its surrogate variable, the equivalent latitude, were found to be important predictors of BTS temperature and permafrost distribution in several areas worldwide (Leverington and Duguay, 1997; Gruber and Hoelzle, 2001; Lewkowicz and Ednie, 2004; Julián and Chueca, 2007). Interactions of PISR and elevation or MAAT have not previously been studied in this context.

Geological factors that might modify topographic and climatic patterns include lithological controls on weathering rates. These influences could however not be considered in the present analysis due to a lack of geological information at the present scale and resolution.

Predictive Performance and the Utility of Spectral Information

Incorporating predictor variables derived from multispectral remote sensing reduced the FPR of the GAM in the study area by one-quarter to one-third from 9.6 per cent (GAM-TA; bootstrap: 10.8%) to 6.0 per cent (GAM-TA-RS; bootstrap: 7.9%), resulting in a much more focused prediction of potential rock glacier areas. Thus, while the remote-sensing model itself is not of practical importance for mapping rock glaciers (FPRs of GAM-RS >40%), spectral data are useful for improving terrain attribute-based models by providing additional explanatory variables that correlate only weakly with terrain attributes.

The reduction of the FPR by adding Landsat ETM+ data to topographic data in a similar study in the San Juan Mountains (Colorado, USA) resulted in more pronounced gains in FPR at a sensitivity of 70 per cent (Brenning, 2009). We attribute this difference to the greater importance of vegetation and hence the NDVI in excluding non-rock glacier areas in the San Juan Mountains. In the present study area, vegetation is virtually absent at elevations that are suitable for rock glacier development.

In the Andes of Santiago and Mendoza, Brenning and Trombotto (2006) achieved an AUROC of 0.84 in rock glacier distribution modelling with a GLM-TA-type model that however includes manually adjusted nonlinear transformations of elevation (representing MAAT) and catchment area. Its FPR at a sensitivity of 70 per cent is approximately 22 per cent. These values are comparable to those achieved in this study with the GLM-TA and GAM-TA on the model domain (Table 4). Other studies presenting empirical or physically motivated models of rock glacier occurrence do not provide comparable measures of model performance (Janke, 2005; Frauenfelder et al., 2008).

Overall, the empirical relationships found in this study may help explore rock glacier distribution in areas where it is currently unknown. Our results indicate that a combination of catchment related and local terrain attributes with the regional climatic trend of MAAT and topoclimatic influences of solar radiation is required for detecting rock glaciers. This topographic and climatic characterisation can be refined using remotely sensed data, especially in the

thermal infrared and, depending on the presence of vegetation in the study area, the NDVI (Brenning, 2009). In the context of permafrost studies using remote sensing and terrain analysis, Leverington and Duguay (1997) and Ødegård et al. (1999) found empirical relationships between TM band 6 and ground thermal conditions. However, in both cases empirical models could be improved only slightly by including the thermal band as an additional predictor. This suggests that the thermal band reflects ground thermal conditions in general without necessarily indicating the presence of ice-rich permafrost, which would be desirable for rock glacier mapping. Taschner and Ranzi (2002) suggest that the thermal band allows us to delineate ground ice underneath a debris cover of less than 50 cm. This may limit the (univariate) utility of band 6 alone for detecting ice-rich permafrost underneath a 2–5-m thick active layer, unless this active layer presents a pronounced thermal offset due to the presence of a coarse blocky layer as on rock glaciers.

Rock glaciers in our data set have, on average, a slightly brighter spectral signal in the TM/ETM+ band 2, which measures reflectance in the green wavelength segment, and/ or other highly correlated spectral bands (especially TM/ETM+ bands 1, 3, 4). The selection of this variable is however not consistent between the bootstrap replications and might be related to the influence of small remnant snow patches on the spectral signal of about ten rock glaciers, especially in Landsat ETM+ 233/79 scene acquired in November 2000 during snowmelt. It is therefore considered a possible artifact.

The present findings have implications for glacier inventories involving debris-covered glaciers. These have similarly weak spectral characteristics (compare Gratton et al., 1990; Taschner and Ranzi, 2002; Brenning, 2009) with some information in the thermal infrared band when the debris cover is thin (Taschner and Ranzi, 2002), but can also be morphometrically characterised in terms of local and catchment-related terrain attributes (Brenning and Trombotto, 2006). However, until now only local slope and curvature variables have been employed in satellite-based glacier inventories (Bishop et al., 2001; Bonk, 2002; Paul et al., 2004; Kargel et al., 2005; Bolch and Kamp, 2006; Bolch et al., 2008). The terrain attributes and classification models applied in this study and by Brenning (2009) provide further research directions for debris-covered glacier mapping.

Nonlinearities and the Utility of the GAM

The presence of nonlinearities in the relationship between predictor variables and rock glacier presence/absence is reflected by our results both analytically in terms of variable selection frequencies and hypothesis tests (Tables 2 and 3), and in a predictive context as expressed by improved AUROC and FPR values of the GAMs compared to the GLMs with the same predictor variables. Though some of the nonlinearities appear to be moderate (Figure 1), or are not significant (Table 2), or are not consistent (Table 3), the

GAM with terrain attributes and remote-sensing variables reduced the FPR by one-quarter to one-third compared to the GLM (Table 4). Nonlinearities would have been more pronounced if the masking based on the unsuitability score had not been applied because this involved nonlinear operations at the cutoff values for elevation, catchment area, and local and catchment slope. Catchment area is particularly known to involve nonlinearities because of the existence of an 'optimal' talus shed size for rock glaciers, beyond which fluvial processes would generally dominate (Brenning and Trombotto, 2006).

The gain in predictive performance related to use of the GAM is comparable to the performance improvement achieved by adding remote-sensing variables to the set of predictors. Using the GAM instead of GLM in a statistical software such as R, however, comes at virtually no extra cost in the analyst's time, while processing of multiple Landsat scenes is relatively labour-intensive.

CONCLUSIONS

This study characterises the topographic and climatic niche of rock glaciers in terms of local and catchment-scale terrain attributes that are related to talus supply, and as a function of solar radiation and MAAT, which are key controls of the energy balance of mountain permafrost. A striking feature that confirms earlier findings of Brenning and Trombotto (2006) is that high solar radiation has a favourable effect on rock glacier occurrence probability at negative regional MAATs, while it has the opposite effect at positive MAATs. While the latter effect is not surprising, the former may relate to reduced creep rates (compare Janke and Frauenfelder, 2008) and meltwater supply at cold, shady high-elevation sites hampering rock glacier formation and growth.

Rock glacier detection in the dry Andes can benefit from the integration of terrain attributes, regional-scale trends of MAAT and remote-sensing data in modern, nonlinear prediction methods such as the GAM. Multispectral Landsat TM/ETM+ improves the false-positive prediction rate of terrain attribute-based classification in the study area by one-quarter to one-third, and the GAM achieves a similar improvement compared to the more widely used GLM or logistic regression. Our results may help improve rock glacier mapping methods and products that are currently required for large areas of the Andes, and they may prove useful in the automatic creation of satellite-based glacier inventories involving a significant portion of debris-covered surfaces (e.g. Bown et al., 2008; Bolch and Kamp, 2006).

ACKNOWLEDGEMENTS

REFERENCES

Azócar GF, Brenning A. 2009. Hydrological and geomorphological significance of rock glaciers in the dry Andes, Chile (27°–33°S). *Permafrost and Periglacial Processes* In press. DOI: 10.1002/ppp.669

Bishop MP, Bonk R, Kamp U, Shroder JF. 2001. Terrain analysis and data modeling for alpine glacier mapping. *Polar Geography* **25**: 182–201.

Bolch T, Kamp U. 2006. Glacier mapping in high mountains using DEMs, Landsat and ASTER data. *Grazer Schriften der Geographie und Raumforschung* **41**: 37–48.

Bolch T, Buchroithner MF, Kunert A, Kamp U. 2008. Automated delineation of debris-covered glaciers based on ASTER data. In *GeoInformation in Europe*, Gomarasca MA (ed.) Proceedings, 27th EARSeL Symposium, June 4–7, 2007, Bozen, Italy. Millpress: Rotterdam, The Netherlands; 403–410.

Bonk R. 2002. Scale-dependent geomorphometric analysis for glacier mapping at Nanga Parbat: GRASS GIS approach. In *Proceedings, Open Source GIS — GRASS Users Conference 2002*, Trento, Italy, 11–13 September 2002. University of Trento: Trento, Italy; 4 pp.

Bown F, Rivera A, Acuña C. 2008. Recent glacier variations at the Aconcagua basin, central Chilean Andes. *Annals of Glaciology* **48**: 43–48.

Brenning A. 2005. Climatic and geomorphological controls of rock glaciers in the Andes of Central Chile: Combining statistical modelling and field mapping. PhD dissertation, Humboldt-Universität zu Berlin. urn:nbn:de:kobv:11-10049648.

Brenning A. 2009. Benchmarking classifiers to optimally integrate terrain analysis and multispectral remote sensing in automatic rock glacier detection. *Remote Sensing of Environment* **113**: 239–247. DOI: 10.1016/j.rse.2008.09.005.

Brenning A, Trombotto D. 2006. Logistic regression modeling of rock glacier and glacier distribution: topographic and climatic controls in the semi-arid Andes. *Geomorphology* **81**: 141–154. DOI: 10.1016/j.geomorph.2006.04.003.

Brenning A, Grasser M, Friend D. 2007. Statistical estimation and generalized additive modeling of rock glacier distribution in the San Juan Mountains, Colorado, USA. *Journal of Geophysical Research* **112**: F02S15. DOI: 10.1029/2006JF000528.

Frauenfelder R, Haeberli W, Hoelzle M. 2003. Rockglacier occurrence and related terrain parameters in a study area of the Eastern Swiss Alps. In *Permafrost, Proceedings of the Eighth International Conference on Permafrost*, 21–25 July 2003, Zürich, Switzerland, Phillips M, Springman SU, Arenson LU (eds). Balkema: Lisse; 253–258.

Frauenfelder R, Schneider B, Kääb A. 2008. Using dynamic modelling to simulate the distribution of rockglaciers. *Geomorphology* **93**: 130–143. DOI: 10.1016/j.geomorph.2006.12.023.

Gratton DJ, Howarth PJ, Marceau DJ. 1990. Combining DEM parameters with Landsat MSS and TM imagery

in a GIS for mountain glacier characterization. *IEEE Transactions on Geoscience and Remote Sensing* **28**: 766–769.

Gruber S, Hoelzle M. 2001. Statistical modeling of mountain permafrost distribution: local calibration and incorporation of remotely sensed data. *Permafrost and Periglacial Processes* **12**: 69–77. DOI: 10.1002/ppp.374

Hall DK, Ormsby JP, Bindschadler RA, Siddalingaiah H. 1987. Characterization of snow and ice reflectance zones on glaciers using Landsat TM data. *Annals of Glaciology* **9**: 104–108.

Hall DK, Foster JL, Salomonson VV. 1995. Development of methods for mapping global snow cover using Moderate Resolution Imaging Spectroradiometer data. *Remote Sensing of Environment* **54**: 127–140.

Hastie TJ, Tibshirani R. 1990. *Generalized Additive Models*. CRC Press: Boca Raton, Florida.

Hjort J, Luoto M. 2006. Modelling patterned ground distribution in Finnish Lapland: An integration of topographical, ground and remote sensing information. *Geografiska Annaler* **88A**: 19–29.

Janke J. 2005. The occurrence of alpine permafrost in the Front Range of Colorado. *Geomorphology* **67**: 375–389. DOI: 10.1016/j.geomorph.2004.11.005.

Janke J, Frauenfelder R. 2008. The relationship between rock glacier and contributing area parameters in the Front Range of Colorado. *Journal of Quaternary Science* **23**: 153–163. DOI: 10.1002/jqs.1133.

Johnson BG, Thackray GD, Van Kirk R. 2007. The effect of topography, latitude, and lithology on rock glacier distribution in the Lemhi Range, central Idaho, USA. *Geomorphology* **91**: 38–50. DOI: 10.1016/j.geomorph.2007.01.023.

Julián A, Chueca J. 2007. Permafrost distribution from BTS measurements (Sierra de Telera, Central Pyrenees, Spain): Assessing the importance of solar radiation in a mid-elevation shaded mountainous area. *Permafrost and Periglacial Processes* **18**: 137–149. DOI: 10.1002/ppp.576.

Kääb A. 2005. Remote Sensing of Mountain Glaciers and Permafrost Creep. Schriftenreihe Physische Geographie 48. University of Zürich: Zürich, Switzerland.

Kargel JS, Abrams MJ, Bishop MP, Bush A, Hamilton G, Jiskoot H, Kääb A, Kieffer HH, Lee EM, Paul F, Rau F, Raup B, Shroder JF, Soltesz D, Stainforth D, Stearns L, Wessels R. 2005. Multispectral imaging contributions to global land ice measurements from space. *Remote Sensing of Environment* **99**: 187–219. DOI: 10.1016/j.rse.2005.07.004.

Koenker R. 2005. *Quantile Regression*. Cambridge University Press: Cambridge, UK.

Leverington DW, Duguay CR. 1997. A neural network method to determine the presence or absence of permafrost near Mayo, Yukon Territory, Canada. *Permafrost and Periglacial Processes* **8**: 205–215.

Lewkowicz AG, Ednie M. 2004. Probability mapping of mountain permafrost using the BTS method, Wolf Creek, Yukon Territory, Canada. *Permafrost and Periglacial Processes* **15**: 67–80. DOI: 10.1002/ppp.480.

Luoto M, Hjort J. 2005. Evaluation of current statistical approaches for predictive geomorphological mapping. *Geomorphology* **67**: 299–315. DOI: 10.1016/j.geomorph.2004.10.006.

Ødegård RS, Isaksen K, Mastervik M, Billdal L, Engler M, Sollid JL. 1999. Comparison of BTS and Landsat TM data from Jotunheimen, southern Norway. *Norsk Geografisk Tidsskrift* **53**: 226–233.

Paul F, Huggel C, Kääb A. 2004. Combining satellite multispectral image data and a digital elevation model for mapping of debris-covered glaciers. *Remote Sensing of Environment* **89**: 510–518. DOI: 10.1016/j.rse.2003.11.007.

Sidjak RW, Wheate RD. 1999. Glacier mapping of the Illecillewaet icefield, British Columbia, Canada, using Landsat TM and digital elevation data. *International Journal of Remote Sensing* **20**: 273–284. DOI: 10.1016/j.rse.2004.12.012.

Taschner S, Ranzi R. 2002. Comparing the opportunities of Landsat-TM and Aster data for monitoring a debris covered glacier in the Italian Alps within the GLIMS project. *IEEE Geoscience and Remote Sensing Symposium* **2**: 1044–1046.

Wahrhaftig WB, Cox A. 1959. Rock glaciers in the Alaska Range. *Geological Society of America Bulletin* **70**: 383–436.

Williams RS, Hall DK, Benson CS. 1991. Analysis of glacier facies using satellite techniques. *Journal of Glaciology* **37**: 120–128.